Training a Multi-Layer Photonic Spiking Neural Network With Modified Supervised Learning Algorithm Based on Photonic STDP

Shuiying Xiang, Zhenxing Ren, Yahui Zhang, Ziwei Song, Xingxing Guo, Genquan Han, and Yue Hao

***Abstract*—We propose a framework for hardware architecture and learning algorithm co-design of multi-layer photonic spiking neural network (SNN). The vertical-cavity surface-emitting laser with an embedded saturable absorber (VCSEL-SA) which contains two polarization-resolved modes is employed as a spiking neuron. The connection between two identical polarization modes is considered as the excitatory synapse, whereas the connection between two orthogonal polarization modes is regarded as the inhibitory synapse. The physical model of the photonic spiking neuron is derived based on the combination of spin-flip model and Yamada model. The photonic spike timing dependent plasticity (STDP) is applied to design a hardware-friendly biologically plausible supervised learning algorithm for a multi-layer photonic SNN. Thanks to the polarization mode competition effect in the VCSEL-SA, the proposed neuromorphic network is capable of solving the classical XOR problem. The effect of physical parameters of photonic neuron on the training convergence is also considered. We further extend the multi-layer photonic SNN to realize other logic learning tasks. To the best of our knowledge, such a modified supervised learning algorithm dedicated for a multi-layer photonic SNN has not yet been reported, which is interesting for spiking learning of neuromorphic photonics.**

***Index Terms*—Photonic spiking neural network, vertical-cavity surface-emitting lasers, multi-layer spiking neural network, spike timing dependent plasticity, supervised learning.**

I. Introduction

RECENT advances in the development of artificial neural networks (ANNs) including the convolutional neural network, recursive neural network and other deep neural networks significantly extend the capability of artificial intelligence in various tasks such as image recognition, natural language processing, self-driving cars, etc. [1]–[3]. However, the operation of these ANNs with the modern computer systems based on the conventional von Neumann architecture is seriously restricted due to the fact that the memory and central processing units are physically separated. Brain-inspired neuromorphic computing based on a non-von Neumann architecture becomes an emerging field for the efficient implementation of artificial intelligence [4]–[6].

Spiking neural network (SNN) is one of the most widely studied and well-developed neuromorphic architecture, and is typically considered as the third generation of ANN [7]. Similar to biological neurons, spiking neurons use spikes to encode information [8]–[10]. The spike timing dependent plasticity (STDP), which is a widely observed phenomenon in biological experiments [11]–[13], is a foundation for designing training algorithms for SNN. In recent years, various learning algorithms have been designed to train the SNNs [14]–[24]. Besides, numerous electronic synapses and neurons, as well as neuromorphic circuits enable various neural computing functions have been developed for the hardware implementations of SNNs [4]–[6], [25]–[32] (for more details please refer to reviews presented in Refs. [4]–[6]). However, these electronic approaches suffer from different drawbacks in the forms of energy-efficiency and speed.

Neuromorphic photonics merges the unique advantages of both photonics techniques and neuromorphic computing, and becomes a hot topic in recent years, but is still in its infancy. In a photonic neuromorphic computing system, the photonic synapses and photonic spiking neurons are triggered by photonic signals, which inherently exhibit enhanced operation speed. In recent years, a considerable number of photonic neurons, photonic synapses, as well as photonic neural computing functions have been proposed and demonstrated both numerically and experimentally [33]–[65]. For instance, J. Feldman *et al.* fabricated an all-optical nanophotonic chip consisting of four neurons and sixty synapses capable of unsupervised and supervised learning [55]. They experimentally demonstrated pattern recognition in a single-layer photonic SNN. S. Barbay *et al.* fabricated a vertical-cavity micropillar lasers with integrated saturable absorber and demonstrated that it could act as a leaky integrate-and-fire (LIF) neuron [37], [58]. They further predicted the potential to build integrated circuits and networks [58]. Note, vertical-cavity surface-emitting lasers (VCSELs) have been widely employed

Manuscript received December 24, 2019; revised April 22, 2020 and June 24, 2020; accepted June 25, 2020. Date of publication July 6, 2020; date of current version July 10, 2020. This work was supported in part by the National Key Research and Development Program of China under Grant 2018YFB2200500, in part by the National Natural Science Foundation of China under Grants 61974177, 61674119. *(Corresponding author: Shuiying Xiang.)*

Shuiying Xiang is with the State Key Laboratory of Integrated Service Networks, Xidian University, Xi'an 710071, China, and also with the State Key Discipline Laboratory of Wide Bandgap Semiconductor Technology, School of Microelectronics, Xidian University, Xi'an 710071, China (e-mail: jxxsy@126.com).

Zhenxing Ren, Yahui Zhang, Ziwei Song, and Xingxing Guo are with the State Key Laboratory of Integrated Service Networks, Xidian University, Xi'an 710071, China (e-mail: 584401206@qq.com; 18332551054@163.com; 1064971297@qq.com; 1966461830@qq.com).

Genquan Han and Yue Hao are with the State Key Discipline Laboratory of Wide Bandgap Semiconductor Technology, School of Microelectronics, Xidian University, Xi'an 710071, China (e-mail: gqhan@xidian.edu.cn; yhao@xidian.edu.cn).

Color versions of one or more of the figures in this article are available online at https://ieeexplore.ieee.org.

Digital Object Identifier 10.1109/JSTQE.2020.3005589

as the photonic neurons due to the advantages of low power consumption, low cost, and easy implementation of large-scale integration [33], [34], [36], [37], [42], [44]–[48], [54], [57]–[59], [61]–[65]. In our previous works, we designed unsupervised and supervised learning algorithms for a single-layer photonic SNN, and numerically realized the spike timing recognition and spike sequence learning [57], [65].Very recently, A. Hurtado *et al.* reported a first experimental demonstration of coincidence detection and pattern recognition with a spiking VCSEL neuron [64]. Meanwhile, the inhibitory dynamics of photonic neuron has attracted lots of attentions as the inhibition is difficult to realize in the optical domain due to the lack of negative optical pulse [42], [46], [54], [61]. The inhibitory dynamics was further exploited to implement the XOR operation at a single step by using a single VCSEL with an embedded saturable absorber (VCSEL-SA) [61]. Despite the rapid development of the photonic neuromorphic systems in recent years, the previously reported photonic SNNs were mainly limited to single-layer network, or considered simple neural functions [55], [57], [58], [60]–[65]. A multi-layer photonic SNN with dedicated hardware-friendly learning algorithm still remains a significant challenge [63].

In this paper, we attempt to design a modified biologically plausible supervised learning algorithm to train a multi-layer photonic SNN consisting of VCSELs-SA. Both x-polarization (XP) and y-polarization (YP) modes could exist in the VCSEL-SA. The synaptic connections between the XP and XP (YP) modes of two adjacent photonic neurons are considered as excitatory (inhibitory) connection. A classical XOR problem is employed as the benchmark test. The main contributions: firstly, a hardware architecture of multi-layer photonic SNN based on VCSELs-SA is proposed for the first time, and a unified computation model of the multi-layer photonic SNN is derived. Secondly, a hardware-friendly supervised learning algorithm dedicated for the multi-layer photonic SNN is designed, which specifically takes into account both the excitatory XP connection and inhibitory YP connection. Thirdly, we further examine the effects of device variations on the training convergence. The rest of this paper is organized as follows. In Section II, the system architecture of the proposed multi-layer photonic SNN is described. Besides, the theoretical model of photonic SNN is derived based on the combination of Yamada model and spin flip model (SFM). The modified supervised learning algorithm for updating both XP and YP connections weights is presented. In Section III, the inhibitory dynamics of photonic spiking neurons is analyzed. Then, the training performance of the XOR learning with the modified supervised learning algorithm is examined carefully. The effects of different bias current, small frequency detuning and encoding time jitter are examined. The adaptation to other logic learning tasks is discussed. Finally, conclusions are drawn in Section IV.

II. Theoryand Model

A. Architecture of the Proposed Multi-Layer Photonic SNN

In order to solve the nonlinear classification problem, we build a multi-layer photonic SNN based on the excitable VCSELs-SA, as shown in Fig. 1.

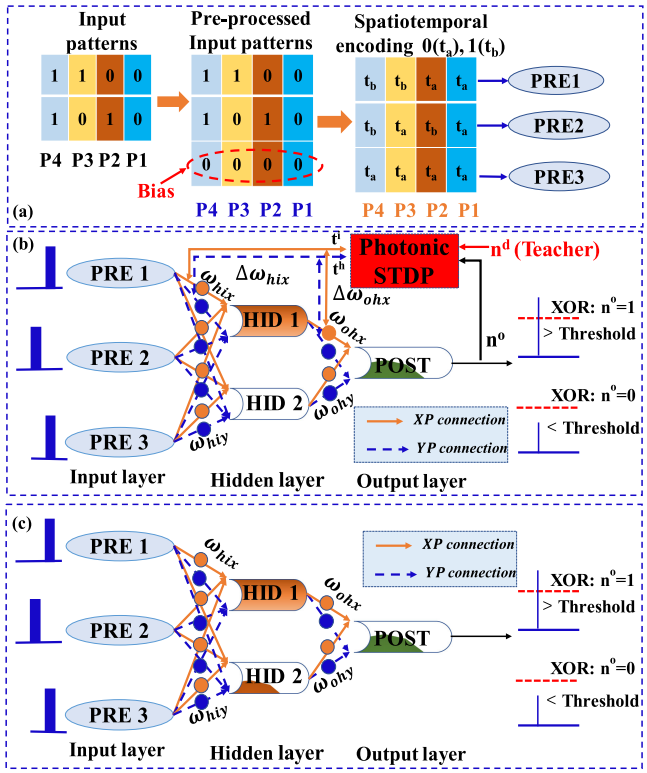

Fig. 1. The architecture of the proposed multi-layer photonic SNN for solving the XOR task, (a) the encoding process, (b) the training process, (c) the inference process. P1-P4: four input patterns, PRE1-PRE3: three VCSELs-SA in the input layer, HID1-HID2: two VCSELs-SA in the hidden layer, POST: a VCSEL-SA in the output layer. The solid orange line with one-way arrow: the optical path of the XP connection (from XP mode to XP mode), the dashed blue line with one-way arrow: the optical path of the YP connection (from XP mode to YP mode), the orange dots and the blue dots represent the weighting devices such as controllable attenuator and amplifier. $\omega_{hix,ohx}$ and $\omega_{hiy,ohy}$ represent connection weights. Photonic STDP is used to control the weight change through external feedback. $\Delta\omega_{hix,ohx}$ means the weight change. $n^o = 0$: POST emits no spike. $n^o = 1$: POST emits a spike.

Here, 00, 01, 10, and 11 are four input patterns. An additional bias bit (0) is added for each pattern. With the bias bit as a time reference, faster convergence can be achieved as the patterns 00 and 11 can be better distinguished [14], [66], and the architecture and algorithm can be easily adapted to other logic tasks. Then, the pre-processed input patterns feeding to the XOR learning network are 000, 010, 100, and 110. For convenience, the original input patterns and the pre-processed input patterns with bias bit are both denoted as P1, P2, P3 and P4, respectively. Similar to [14], [66], [67], the bit 0 (1) is temporally encoded as a rectangle pulse with central timing at $t_a = 30$ ns ($t_b = 50$ ns), as presented in Fig. 1(a). Here, the temporal duration of the rectangle pulse is 5 ns. The reason for using the temporal encoding paradigm is as follows. On the one hand, there is increasing evidence shows the neural system conveys information via the precise timing of spikes [8], [9]. On the other hand, the spike encoding should be co-designed with the training algorithm. The photonic STDP rule incorporated into the training algorithm updates the weight according to the difference between the precise timing of pre- and post-synaptic spikes. After that, the rectangle pulses are then injected into the XP mode of three VCSELs-SA (PRE1 and

PRE2 for signal bits, PRE3 for bias bit), respectively, to perform temporal spike encoding. The XP output of the input layer is then injected into both the XP and YP modes of two VCSELs-SA in the hidden layer. Here, the XP (YP) connection, i.e., from XP mode to XP (YP) mode, emulates the excitatory (inhibitory) synapse. The synaptic weight is represented by the optical power of the injected light, and can be adjusted with weighting elements such as controllable amplifier and attenuator. These weighting elements can be directly inserted into the optical path of XP and YP connections as denoted in Figs. 1(b) and (c). Similarly, the XP output of the hidden layer is then propagated to both the XP and YP modes of the VCSEL-SA in the output layer. The target is encoded as binary output, i.e., with or without spike emission. For P1 and P4, the XOR result is 0, corresponding to no spike emission for the POST, i.e., $n_1^d = n_4^d = 0$. While for P2 and P3, the XOR result is 1, that is, the POST is allowed to emit a spike, i.e., $n_2^d = n_3^d = 1$.

During training process, as shown in Fig. 1(b), the teacher signal n^d, the actual output spike number and timing, as well as the spike timing of XP mode in the input and hidden layers are used for calculating the weight update amount according to the photonic STDP. In a practical physical system, the weighting stage and the plasticity stage can be separated, and the photonic STDP module can be used to control the weight change through external feedback [35], [40], [68]. There are 16 individual weights had to be adjusted. Only positive weights are allowed, and the maximum weight is set to be 0.23 to prevent lasers from receiving too strong injected light. After training convergence, the weights can be fixed and used for the inference process as displayed in Fig. 1(c). Note, given the technologies available, we think it may be more realistic to adopt an ex-situ learning approach for the training process. Nevertheless, thanks to the advanced photonic integration technology, it is promising to build a hardware multi-layer photonic SNN consisting of VCSEL-SA for realizing the inference process [58], [64].

B. Model of Photonic Neuron: Rate Equations of VCSEL-SA With Two Polarization-Resolved Modes

To mimic a LIF neuron, the VCSEL-SA is employed here. The rate equations are derived based on the combination of Yamada model and SFM for a VCSEL-SA with two polarization modes [48], [54], [69]–[71]:

$$\begin{aligned}\frac{dF_{\mathrm{ix},hx,ox}}{dt} &= \frac{1}{2}(1+i\alpha)[(D_1+D_2-1)F_{\mathrm{ix},hx,ox} \\ &\quad + i(d_1+d_2)F_{\mathrm{iy},hy,oy}] \\ &\quad - (\varepsilon_a+i\varepsilon_p)F_{\mathrm{ix},hx,ox} + k_{\mathrm{e}ix}F_{eix}(t)e^{i2\pi\Delta f_{eix}t} \\ &\quad + \sum_{i=1}^{3}\omega_{hix}F_{ix}(t-\tau)e^{i(2\pi\Delta f_{hi}t-\phi_0)} \\ &\quad + \sum_{h=4}^{5}\omega_{ohx}F_{hx}(t-\tau)e^{i(2\pi\Delta f_{oh}t-\phi_0)} \qquad (1)\end{aligned}$$

$$\begin{aligned}\frac{dF_{\mathrm{iy},hy,oy}}{dt} &= \frac{1}{2}(1+i\alpha)[(D_1+D_2-1)F_{\mathrm{iy},hy,oy} \\ &\quad - i(d_1+d_2)F_{\mathrm{ix},hx,ox}] \\ &\quad + (\varepsilon_a+i\varepsilon_p)F_{\mathrm{iy},hy,oy} + \sum_{i=1}^{3}\omega_{hiy}F_{ix}(t-\tau)e^{i(2\pi\Delta f_{hi}t-\phi_0)} \\ &\quad + \sum_{h=4}^{5}\omega_{ohy}F_{hx}(t-\tau)e^{i(2\pi\Delta f_{oh}t-\phi_0)} \qquad (2)\end{aligned}$$

$$\begin{aligned}\dot{D}_{1,2} &= \gamma_{1,2}\Big[\mu_{1,2} - D_{1,2} - \frac{1}{2}a_{1,2}(D_{1,2}+d_{1,2})\,|F_{\mathrm{ix},hx,ox} \\ &\quad + iF_{\mathrm{iy},hy,oy}|^2 \\ &\quad - \frac{1}{2}a_{1,2}(D_{1,2}-d_{1,2})|F_{\mathrm{ix},hx,ox} - iF_{\mathrm{iy},hy,oy}|^2 + c_{12,21}D_{2,1}\Big] \qquad (3)\end{aligned}$$

$$\begin{aligned}\dot{d}_{1,2} &= -\gamma_{s1,2}d_{1,2} - \gamma_{1,2}\Big[\frac{1}{2}a_{1,2}(D_{1,2}+d_{1,2})\,|F_{\mathrm{ix},hx,ox} \\ &\quad + iF_{\mathrm{iy},hy,oy}|^2 \\ &\quad - \frac{1}{2}a_{1,2}(D_{1,2}-d_{1,2})|F_{\mathrm{ix},hx,ox} - iF_{\mathrm{iy},hy,oy}|^2 - c_{12,21}d_{2,1}\Big] \qquad (4)\end{aligned}$$

Where subscripts $i = 1, 2, 3; h = 4, 5; o = 6$ for $F_{x,y}$ denote VCSEL-SA in the input, hidden and output layers, respectively. The subscripts 1 and 2 for *D* and *d* represent the gain and saturable absorber regions, respectively. $F_{x,y}$ represent the slowly varying complex amplitudes of XP and YP modes. D accounts for the total carrier inversion between the conduction and valence bands related to the transparency carrier density. d denotes the carrier inversions with opposite spin orientations. The third term in Eq. (1) represents the external stimulation for the XP mode and exists only for VCSELs-SA in the input layer, where $F_{eix}(t)$is the external stimulating rectangle pulse, $k_{\mathrm{e}ix} = 0.5$ is the stimuli strength, and $\Delta f_{eix}$is frequency detuning. The last two terms in Eq. (1) (Eq. (2)) denote the injection for the XP (YP) mode for the hidden and output layers, respectively. $\tau = 1$ ns denotes transmission delay, ϕ_0 represents an initial phase difference. For simplicity, we consider $\phi_0 = 0$. $\omega_{hix,ohx}$ and $\omega_{hiy,ohy}$ represent connection weights (synapse strength) and are initialized to random values between 0 and 0.23. $\Delta f_{hi,oh}$mean the frequency detuning between VCSELs-SA belong to different layers. ε_a (ε_p) denotes the amplitude (phase) anisotropy. $\varepsilon_p = \gamma_p/k$, where γ_p means the birefringence, and k is the cavity decay rate. The terms $c_{12}D_2$ and $c_{21}D_1$ in Eqs. (3–4) account for the carrier diffusion. α is the linewidth enhancement factor. The rate equations are represented by a dimensionless form, and the time is measured in units of k^{-1}.

In simulations, we consider the following parameters [48], [54], [71]: $\alpha = 3, \varepsilon_a = 0, \gamma_p = 15\ \mathrm{ns}^{-1}, k = 390\ \mathrm{ns}^{-1}, \Delta f_{eix} = \Delta f_{hi,oh} = 0$ GHz, $c_{12} = 2.84 \times 10^{-2}$, $c_{21} = 1.91$, $\beta_{sp} = 0$. The other parameters for all the VCSELs-SA are identical and are presented in Table I. We numerically solve the rate equations using fourth-order Runge-Kutta method. The intensities are calculated by $I_{x,y} = |F_{x,y}|^2$.

TABLE I
VCSEL-SA PARAMETERS [48, 54, 71]

Parameter	Gain region	Absorber region
Bias currents $\mu_{1,2}$	μ_1 =2.1	μ_2 =-6.1
Total carrier decay rates $\gamma_{1,2}$	γ_1=1.09×10^{-3}	γ_2=1.13×10^{-3}
Effective spin-flip rates $\gamma_{s1,s2}$	γ_{s1} =0.25	γ_{s2} =0.25
Differential gains $\alpha_{1,2}$	α_1 =1	α_2 =8.7

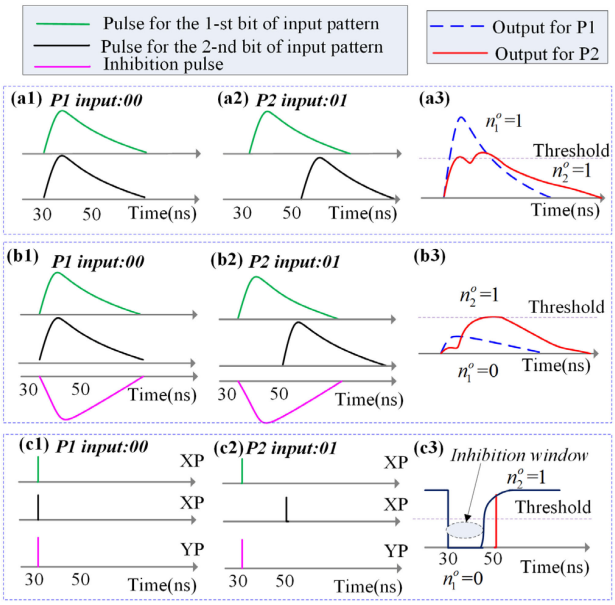

Fig. 2. The schematic diagram of the inhibitory synapse in the XOR learning. P1 (00) and P2 (01) denote two different input patterns. The left (middle) column corresponding to the encoding pulses for the P1 (P2), the right column corresponding to the output for two input patterns. The bit 0 (1) is encoded into a pulse located at 30 ns (50 ns) for each pattern. (a1, a2) without negative pulse as inhibition pulse, (a3) the integrated PSP exceeds the threshold for both P1 and P2, and $n_1^o = n_2^o = 1$, (b1, b2) with an additional negative pulse located at 30 ns acting as the inhibitory pulse, (b3) $n_1^o = 0, n_2^o = 1$, (c1, c2) the signal pulses are injected into the XP mode of VCSEL-SA, an additional pulse located at 30 ns injecting into the YP mode of VCSEL-SA is introduced to emulate the inhibitory behavior, (c3) $n_1^o = 0, n_2^o = 1$.

C. Modified Supervised Learning Algorithm for the Multi-Layer Photonic SNN.

To solve a XOR problem, the negative weight is commonly introduced to produce the inhibition effect in conventional software-based SNN. Here, P1(00) is spatiotemporally encoded as two pulses located at 30 ns. P2(01) is represented by two input patterns located at 30 ns and 50 ns, respectively. As presented in Figs. 2(a1–a2), when without the negative postsynaptic potential (PSP), the integrated PSP exceeds the firing threshold of the output neuron for both P1 and P2 in Figs. 2(a3). Similar to the target encoding scheme, the output can also be encoded as binary output. Namely, when the integrated PSP exceeds the firing threshold, the binary output is 1, otherwise it is 0. Hence, the binary output for both P1 and P2 is $n_1^o = n_2^o = 1$. That is, the XOR task cannot be realized. Fortunately, as presented in Figs. 2(b1–b2), thanks to the introduction of the negative PSP, the binary output for P1 is 0 as illustrated in Fig. 2(b3). The binary output is 1 for P2 because the negative PSP at 30 ns is far away from the second PSP for P2. Namely, $n_1^o = 0, n_2^o = 1$. Hence, the inhibitory PSP enables successful learning of the XOR task. However, it is infeasible to introduce a negative weight in photonic SNN to produce the inhibition behavior, because the weight represented by the injection optical power could not be negative. Here, the polarization mode competition effect in a VCSEL-SA is employed as an alternative to emulate the inhibitory dynamics. As shown in Figs. 2(c1–c2), the signal pulses for P1 and P2 are injected into the XP mode of VCSEL-SA, while the additional pulse located at 30 ns injecting into the YP mode of VCSEL-SA is introduced to emulate the inhibitory behavior. As displayed in Fig. 2(c3), the signal pulse located at 30 ns is within the inhibition window [54], while the signal pulse located at 50 ns is beyond the inhibition window, the VCSEL-SA only emits a spike for P2. Namely, $n_1^o = 0, n_2^o = 1$.

During training process, the weight $\omega_{hix,ohx}$ and $\omega_{hiy,ohy}$ can be adjusted by repeatedly feeding the input patterns to the photonic SNN with supervised learning algorithm. A specific hardware-friendly algorithm is required to adjust the weight for both the excitatory XP connection and the inhibitory YP connection. To this end, we developed a modified supervised learning algorithm based on the Tempotron rule and photonic STDP rule [11], [16], [49]. The weight update amount $\Delta\omega_{hix}$ ($\Delta\omega_{ohx}$) between the XP modes of input and hidden (hidden and output) layers can be calculated as follows,

$$\Delta\omega_{hix} = \begin{cases} \Delta\omega_{STDP}(\Delta t_{hi}), & \text{if } n^d = 1, n^o = 0, \Delta t_{hi} > 0 \\ -\Delta\omega_{STDP}(\Delta t_{hi}), & \text{if } n^d = 0, n^o = 1, \Delta t_{hi} > 0 \end{cases} \quad (5)$$

$$\Delta\omega_{ohx} = \begin{cases} \Delta\omega_{STDP}(\Delta t_{oh}), & \text{if } n^d = 1, n^o = 0, \Delta t_{oh} > 0 \\ -\Delta\omega_{STDP}(\Delta t_{oh}), & \text{if } n^d = 0, n^o = 1, \Delta t_{oh} > 0 \end{cases} \quad (6)$$

Where $\Delta t_{hi} = t_h - t_i$, $\Delta t_{oh} = t_o - t_h$, t_i, t_h and t_o denote the spike timing in the input, hidden and output layers, respectively. $\Delta\omega_{STDP}(\Delta t_{hi,oh})$is introduced as in [49]. $n^d = 1$ ($n^o = 1$) represents the target output (actual output) with spike emission, and $n^d = 0$ ($n^o = 0$)indicates the target output (actual output) without spike emission. Thus, the weight of the excitatory XP connection could be updated by:

$$\omega_{hix,ohx\_new} = \omega_{hix,ohx\_old} + \omega_f \times \Delta\omega_{hix,ohx} \quad (7)$$

For the inhibitory YP connection, the weight update amount is the same as that for the XP connection, but the weight update sign is opposite. Namely, $\Delta\omega_{hiy} = -\Delta\omega_{hix}$, $\Delta\omega_{ohy} = -\Delta\omega_{ohx}$. The corresponding weight can be updated by:

$$\omega_{hiy,ohy\_new} = \omega_{hiy,ohy\_old} - \omega_f \times \Delta\omega_{hix,ohx} \quad (8)$$

$\omega_f = 0.01$ is learning rate.

The weight update process is further illustrated in Fig. 3. Here, four cases of the actual and target outputs are presented. In case(a), $n^d = 0, n^o = 1$, the weight is depressed according to the long term depression (LTD) curve and $\Delta\omega_{STDP}(\Delta t_{hi,oh}) < 0$. For case(b), $n^d = 1, n^o = 0$, t_o is supposed to be equal to the learning window T = 75 ns. The weight is potentiated according to the long term potentiation (LTP) curve and $\Delta\omega_{STDP}(\Delta t_{hi,oh}) > 0$. In cases (c) and (d), for $n^d = 1, n^o = 1$ or $n^d = 0, n^o = 0$, $\Delta\omega_{STDP}(\Delta t_{hi,oh}) = 0$ for all the $\Delta t_{hi,oh}$. Note, to ensure that the spikes from different neurons (from PREs, HIDs and POST neurons) arrive within the same temporal

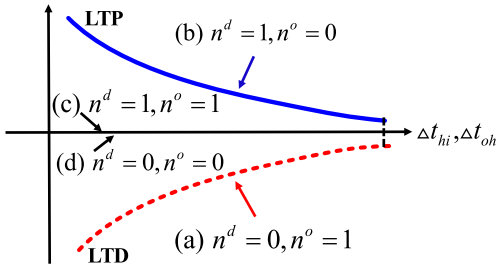

Fig. 3. The schematic diagram of the weight update process for four cases of the actual and target outputs, (a) the weight is updated according to LTD for the case of $n^d=0, n^o=1$, (b) the weight is updated according to LTP for the case of $n^d=1, n^o=0$, (c) the weight is not changed for the case of $n^d=1, n^o=1$, (d) the weight is not changed for the case of $n^d=0, n^o=0$.

Algorithm: Modified Supervised Learning Algorithm Based on Photonic STDP for Multi-Layer Photonic SNN.

1: #Initialization of network constants
$i_{1,2,3}, h_{4,5}, o_6 \leftarrow$ input, hidden, output layer neurons;
constant1 $\leftarrow$ maximum weight; $n^d \leftarrow$ target output;
2: #Initialization of weight $\omega_{hix}, \omega_{hiy}, \omega_{ohx}, \omega_{ohy}$
$\omega_{hix}, \omega_{hiy}, \omega_{ohx}, \omega_{ohy} \leftarrow rand() \times$ constant1;
$\Delta\omega_{hix}, \Delta\omega_{ohx} \leftarrow zeros()$;
3 : While i $<$ training number do
$\omega_{hix} \leftarrow \omega_{hix} + \Delta\omega_{hix}; \omega_{hiy} \leftarrow \omega_{hiy} - \Delta\omega_{hix}$;
$\omega_{ohx} \leftarrow \omega_{ohx} + \Delta\omega_{ohx}; \omega_{ohy} \leftarrow \omega_{ohx} - \Delta\omega_{ohx}$;
$\Delta\omega_{hix}, \Delta\omega_{ohx} \leftarrow zeros()$;
4: Calculate $t_{i1,i2,i3}, t_{h4,h5}, t_{o6}, n^o$;
5: $If\ n^o \neq n_i^d$
$\Delta\omega_{hix} \leftarrow STDPfunction(t_{i1,i2,i3}, t_{h4,h5}, n^o)$;
$\Delta\omega_{ohx} \leftarrow STDPfunction(t_{o6}, t_{h4,h5}, n^o)$;
6: While end

window of the STDP stage, it is suggested to adopt variable optical delay lines to compensate for the transmission delays in practice.

The modified supervised learning algorithm can be summarized as follows.

III. Numerical Results

In this section, we firstly consider the inhibitory dynamics of a VCSEL-SA subject to dual-polarized spike injections. Then the supervised training process is presented. The effect of bias current and frequency detuning on the training convergence is considered. In addition, the robustness to spike encoding time jitter is discussed. At last, we further extend the multi-layer photonic SNN to realize other logic learning tasks with the modified supervised learning algorithm.

A. Inhibitory Dynamics of VCSEL-SA Subject to Dual-Polarized Optical Spike Injection Based on Polarization Mode Competition

At first, we consider a simple photonic SNN consisting of VCSEL-SA1 and VCSEL-SA2 acted as the PREs, VCSEL-SA4 acted as the HID. The external stimulation pulses are injected

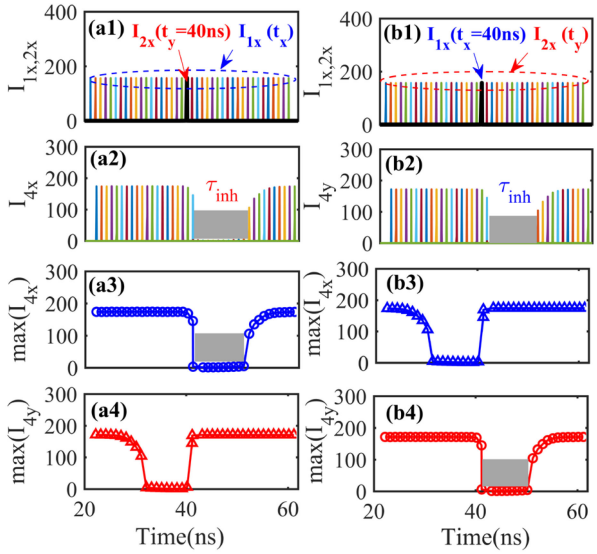

Fig. 4. The inhibitory dynamics of VCSEL-SA subject to dual-polarized spike injections. (a1) I_{1x} for different t_x and I_{2x} for $t_y=40$ ns, t_x is varied from 20 ns to 60 ns, (b1) I_{1x} for $t_x=40$ ns and I_{2x} for different t_y, t_y is varied from 20 ns to 60 ns, (a2) I_{4x} for different t_x, (b2) I_{4y} for different t_y, (a3), (b3) the peak intensities of I_{4x} for different t_x, (a4), (b4) the peak intensities of I_{4y} for different t_y. The maximum weight is used $\omega_{41x}=\omega_{42y}=0.23.\tau_{\rm inh}$ denotes inhibition window.

into the XP modes of VCSEL-SA1 and VCSEL-SA2. Then the XP output of VCSEL-SA1 is injected into the XP mode of VCSEL-SA4 to act as excitatory synapse, while the XP output of VCSEL-SA2 is injected into the YP mode of the VCSEL-SA4 to serve as inhibitory synapse.

Two different input conditions are considered. As shown in Fig. 4 (a1), t_x which denotes the timing of spike generated by VCSEL-SA1 (I_{1x})is varied from 20 ns to 60 ns. The timing of the spike generated by VCSEL-SA2 (I_{2x}) is fixed at $t_y=40$ ns. I_{4x} for different t_x is presented in Fig. 4(a2). The corresponding peak intensities of I_{4x} and I_{4y} are presented in Figs. 4(a3) and (a4). It can be seen that, when $t_x < t_y$, I_{4x} is not affected by the spike injected into the YP mode (I_{2x}), and reaches its maximum, while the YP response is inhibited. On the other hand, when $t_x \geq t_y$, the response dynamics is quite different. For $40\ \text{ns} \leq \text{t}_\text{x} < 51\ \text{ns}$, as the carrier number is reduced substantially via the stimulated radiation process due to the injection in the YP mode, the peak intensity of I_{4x} is very small. After that, the peak intensity of I_{4x} is increased gradually due to the carrier recovery. For the other input condition, as presented in Fig. 4(b1), I_{1x} is fixed at $t_x=40$ ns, while t_y is varied from 20 ns to 60 ns. I_{4y} for different $t_y$is presented in Fig. 4 (b2). The peak intensities of I_{4x} and I_{4y} are presented in Figs. 4(b3) and (b4). Obviously, similar inhibition behavior can be observed in the YP mode of VCSEL-SA4. Here, the time window associated with the inhibition of XP spike can be referred to as inhibition window, which is linked to the weight, bias current, and carrier recovery dynamics.

During the training process, the excitatory XP connections and inhibitory YP connections are more complex than the cases presented in Fig. 4, and the weight is different for each training epoch. For a given VCSEL-SA, as long as the weight for at least one of the XP connections and one of the YP connections are not

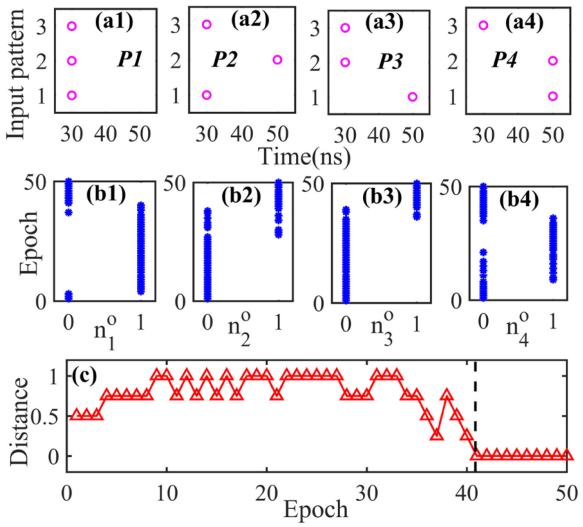

Fig. 5. Training process for the XOR task. (a1)-(a4) the four input patterns corresponding to P1, P2, P3 and P4, respectively, (b1)-(b4) the evolution of n_P^o, during the training process corresponding to P1, P2, P3 and P4, respectively, $n_P^o = 0$ ($n_P^o = 1$) represents without (with) spike emission, (c) the Distance as a function of training epoch.

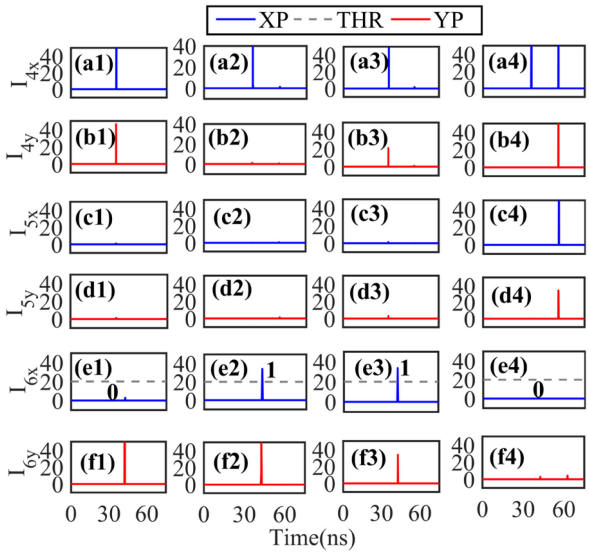

Fig. 6. The temporal output of two polarization-resolved modes of the VCSEL-SA in the hidden and output layers for the four patterns. From left to right: for P1, P2, P3, and P4.

zero, such inhibition behavior will exist due to the polarization mode competition effect in that VCSEL-SA.

B. Supervised Training the Multi-Layer Photonic SNN for Solving the XOR Problem.

To evaluate quantitatively the training performance, we further define a distance as follows,

$$\text{Distance} = \frac{1}{N}\sum_{P=1}^{N}\left(n_P^d - n_P^o\right)^2 \tag{9}$$

Where N is the number of patterns, n_P^d and n_P^o denote the spike emission output for the desired and actual outputs for the P-*th* pattern. When there is no spike emission, $n_P^{d,o} = 0$, otherwise, $n_P^{d,o} = 1$. Hence, when the Distance is reduced to 0, successful learning is achieved.

Next, the training process for four different patterns is presented in Fig. 5. It can be seen that, with the designed supervised learning algorithm to adjust the synpatic weight for both excitatory XP connection and inhibitory YP connection, the targets for all the patterns are achieved after about 40 training epochs. The Distance is reduced to 0 after training convergence.The output spikes of XP and YP modes for the VCSELs-SA 4 and 5 (HID), and for VCSEL-SA 6 (POST) after the training convergence are presented in Fig. 6. It is verified that, the XOR result is excatly stored in the form of spike emission of the XP mode of POST. More precisely, for P1 or P4, the POST emits no spike in the XP mode, i.e., $n_1^o = n_4^o = 0$. While for P2 and P3, the POST emits spike in the XP mode, i.e., $n_2^o = n_3^o = 1$. These outputs conincide with the target outputs, indicating successful XOR learning.

To present more insight into the training process, the evolution of the weight during traning is presented in Figs. 7(a) and (b). We can see that some weights are potentiated while others are

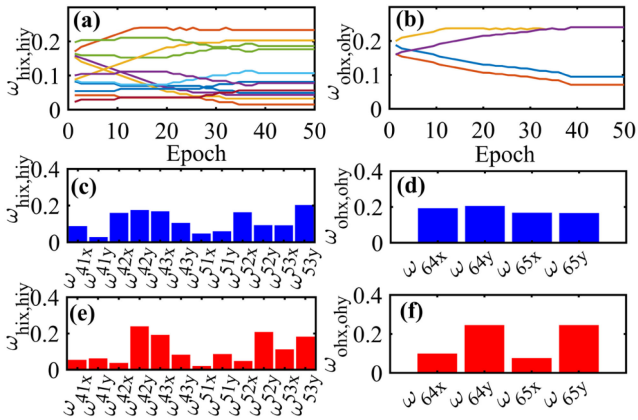

Fig. 7. (a), (b) The evolution of weight, (c), (d) weight distribution before training, (e), (f) weight distribution after training. The left (right) column corresponds to the weight between the input and hidden layers (between the hidden and output layers).

depressed. After the training process is converged, the weights are not updated. Furthermore, the weight distributions before and after training convergence are also presented in Figs. 7(c–f). Obviouly, the weight distribution is greatly modified by the supervised training process.

Subsequently, we also discuss the dependence of the convergence performance on the parameters. Here, the initial weights are the same for different cases. The effect of bias current on the Distance is presented in Fig. 8(a). It can be seen that, the training process can be converged for all the considered cases of μ_1, indicating that the training convergence can be achieved for different bias currents. Moreover, to explore the device variations on the training performance, we also consider a more practical situation that the bias currents of different VCSELs-SA are slightly different. For the case of $\mu_1 = \mu_{set}$, that is, the bias currents of six VCSELs-SA are slightly different, it is clearly that

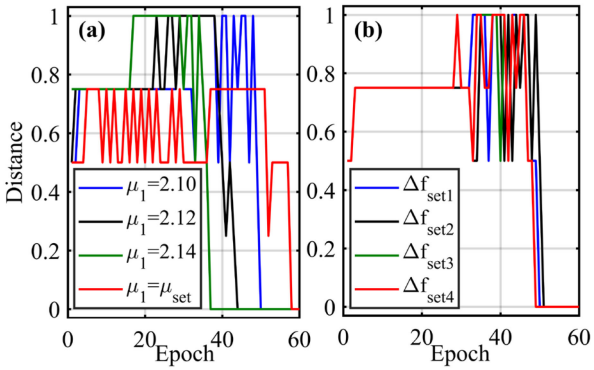

Fig. 8. The Distance as a function of training epoch for different bias current conditions, $\mu_{set} = [2.09, 2.1, 2.11, 2.12, 2.13, 2.14]$, $\Delta f_{set1} = [-5, 0, 0, 0, 0]$ GHz, $\Delta f_{set2} = [-5, 5, 0, 0, 0]$ GHz, $\Delta f_{set3} = [-2, 0, 2, 4, 5]$ GHz, $\Delta f_{set4} = [-5, -2, 0, 2, 4]$GHz.

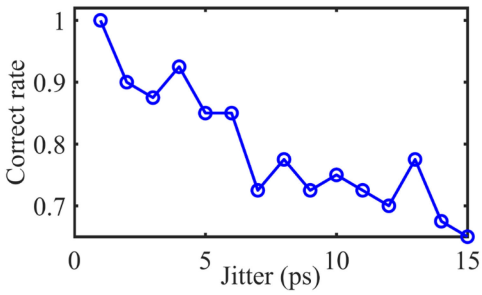

Fig. 9. The correct rate of the inference process as a function of time jitter.

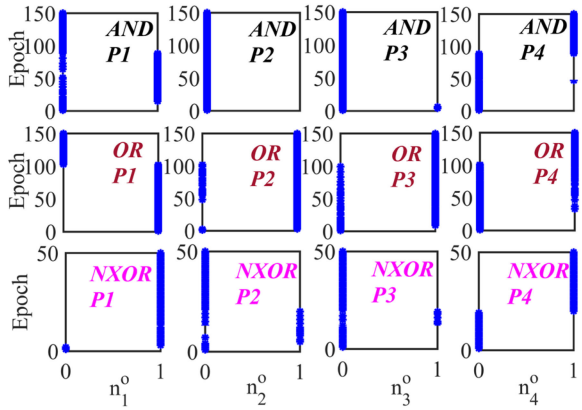

Fig. 10. The training process of four patterns for AND (the top row), OR (the middle row) and NXOR (the bottom row) learning task.

TABLE II
TRUTH TABLE

Pattern	AND (n^d)	OR(n^d)	NXOR(n^d)
P1(00)	0	0	1
P2(01)	0	1	0
P3(10)	0	1	0
P4(11)	1	1	1

the convergence can still be obtained. Similarly, the Distance for different frequency detuning is presented in Fig. 8(b). For convince, we introduce $\Delta f_{set} = [\Delta f_{12}, \Delta f_{13}, \Delta f_{14}, \Delta f_{15}, \Delta f_{16}]$. In this case, the five frequency detuning values can be freely tuned, and the frequency detuning $\Delta f_{hi,oh}$ can be calculated with Δf_{set}. For instance, $\Delta f_{56} = \Delta f_{16} - \Delta f_{15}$. We can see that, for the four cases of Δf_{set}, the training convergence can still be achieved when small frequency detuning is introduced. Consequently, the designed supervised learning algorithm is immune to slight device variations such as bias current fluctuations and small frequency detuning, which is highly desirable for the practical hardware implementation for the multi-layer photonic SNN.

Next, we examine the robustness of an inference process. We consider the time jitter exists in the temporally encoding process. Here, the randomly selected time jitter is added to t_a and t_b. The correct rate as a function of the time jitter is presented in Fig. 9. Here, to obtain statistical significance of the inference accurate rate, we run the test process 50 times for each time jitter. As shown in Fig. 9, the correct rate is above 0.8 when the time jitter is less than 6 picoseconds. With the further increase of time jitter, the correct rate is decreased. That is to say, the inference process is robust to small time jitter.

We also performed similar calculations for $t_b = 40$ ns and $t_b = 45$ ns. It is found that, the XOR learning can still be realized (not shown here). Actually, we find that the XOR learning can be achieved provided the difference between t_a and t_b is sufficiently large. We suggest using time difference greater than the inhibition window so as to make the signal spikes normally propagate into the network. Otherwise, one of the bits would be directly inhibited once they are injected into the hidden layer due to the inhibition dynamics of VCSEL-SA. Besides, we also considered the case by adopting bit 1 as the bias. It is found that, when $t_a = 50$ ns and $t_b = 30$ ns, the XOR learning can also be achieved (not shown here). Hence, the spike timing can be widely tunable during the encoding process.

Without loss of generality, we further extend the multi-layer photonic SNN to solve other logic tasks with the modified supervised learning algorithm. The training process for four patterns for solving the AND, OR and NXOR tasks is presented in Fig. 10. Here, the bias bit and the temporal encoding timings are identical to those used in Fig. 5. The truth table (n^d) for the three logic tasks is presented in Table II. We can see that the actual spike output exactly coincides with the target output. More precisely, when there is no spike emission in the XP mode of VCSEL-SA6 (POST) for a given pattern, i.e., $n^o = 0$, the target output is 0. On the contrary, when the XP mode of VCSEL-SA6 emits a spike for a specific pattern, the target output is exactly 1 as presented in the truth table. Hence, the modified supervised learning algorithm dedicated for the multi-layer photonic SNN can easily adapt to these logic learning tasks.

IV. CONCLUSION

In summary, we proposed to build a multi-layer photonic SNN based on excitable VCSELs-SA and developed a modified biologically plausible supervised learning algorithm based on

photonic STDP rule. The classical XOR task is employed as a benchmark test. The numerical simulations show that, the modified supervised learning algorithm incorporating both excitatory XP and inhibitory YP connections is capable of solving the XOR learning. Besides, the training convergence could be achieved even for VCSELs-SA with slightly different bias currents and small frequency detuning. Consequently, the designed supervised learning algorithm is immune to device variations to some degree. Furthermore, the inference process is robust to small time jitter.

To the best of our knowledge, such multi-layer photonic SNN consisting of excitable VCSELs-SA has not yet been reported. Moreover, this is the first development of a dedicated hardware-friendly modified supervised learning algorithm for a multi-layer photonic SNN. Note that, the present study is concentrated on the numerical simulation of the multi-layer photonic SNN, which may motivate further experimental demonstration of hardware multi-layer photonic SNN, and is expected to pave the way for hardware-algorithm co-design of photonic neuromorphic network.

REFERENCES

[1] M. I. Jordan and M. I. Jordan, "Machine learning: Trends, perspectives, and prospects," *Science*, vol. 349, no. 6245, pp. 255–260, Jul. 2015.

[2] D. Silver *et al.*, "Mastering the game of Go with deep neural networks and tree search," *Nature*, vol. 529, pp. 484–489, Jan. 2016.

[3] D. Silver *et al.*, "Mastering the game of Go without human knowledge," *Nature*, vol. 550, pp. 354–359, Oct. 2017

[4] R. A. Nawrocki, R. M. Voyles, and S. E. Shaheen, "A mini review of neuromorphic architectures and implementations," *IEEE T. Electron Dev.*, vol. 63, no. 10, pp. 3819–3829, Aug. 2016.

[5] C. D. Schuman *et al.*, "A survey of neuromorphic computing and neural networks in hardware," 2017. [Online]. Available: https://arxiv.org/abs/1705.06963

[6] K. Roy, A. Jaiswal, and P. Panda, "Towards spike-based machine intelligence with neuromorphic computing," *Nature*, vol. 575, pp. 607–617, Nov. 2019.

[7] W. Maass, "Networks of spiking neurons: The third generation of neural network models," *Neural Netw.*, vol. 10, no. 9, pp. 1659–1671, Dec. 1997.

[8] Z. F. Mainen and T. J. Sejnowski, "Reliability of spike timing in neocortical neurons," *Science*, vol. 268, no. 5216, pp. 1503–1506, Jul. 1995.

[9] J. Gautrais and S. Thorpe, "Rate coding versus temporal order coding: A theoretical approach," *Biosystems*, vol. 48, nos. 1-3, pp. 57–65, 1998.

[10] T. Gollisch and M. Meister, "Rapid neural coding in the retina with relative spike latencies," *Science*, vol. 319, no. 5866, pp. 1108–1111, Feb. 2008.

[11] G. Bi and M. Poo, "Synaptic modifications in cultured hippocampal neurons: Dependence on spike timing, synaptic strength, and postsynaptic cell type," *J. Neurosci.*, vol. 18, no. 24, pp. 10464–10472, Dec. 1998.

[12] L. F. Abbott and S. B. Nelson, "Synaptic plasticity: Taming the beast," *Nat. Neurosci.*, vol. 3, pp. 1178–1183, Nov. 2000.

[13] G. Q. Bi and M. M. Poo, "Synaptic modification by correlated activity: Hebb's postulate revisited," *Annu. Rev. Neurosci.*, vol. 24, pp. 139–166, Mar. 2001.

[14] S. M. Bohte, J. N. Kok, and H. La Poutre, "Error-backpropagation in temporally encoded networks of spiking neurons," *Neurocomputing*, vol. 48, no. 1, pp. 17–37, 2002.

[15] R. Guyonneau, R. VanRullen, and S. J. Thorpe, "Neurons tune to the earliest spikes through STDP," *Neural Comput.*, vol. 17, no. 4, pp. 859–879, Apr. 2005.

[16] R. Gütig and H. Sompolinsky, "The tempotron: A neuron that learns spike timing-based decisions," *Nat. Neurosci.*, vol. 9, no. 3, pp. 420–428, Feb. 2006.

[17] T. Masquelier, R. Guyonneau, and S. J. Thorpe, "Spike timing dependent plasticity finds the start of repeating patterns in continuous spike trains," *PloS one*, vol. 3, no. 1, Jan. 2008, Paper e1377.

[18] F. Ponulak and A. Kasiński, "Supervised learning in spiking neural networks with ReSuMe: Sequence learning, classification, and spike shifting." *Neural Comput.*, vol. 22, no. 2, pp. 467–510, Feb. 2010.

[19] A. Mohemmed, S. Schliebs, S. Matsuda, and N. Kasabov, "Span: Spike pattern association neuron for learning spatiotemporal spike patterns," *Int. J. Neural Syst.*, vol. 22, no. 04, 2012, Art. no. 1250012.

[20] I. Sporea and A. Grüning, "Supervised learning in multilayer spiking neural networks," *Neural Comput.*, vol. 25, no. 2, pp. 473–509, 2013.

[21] P. U. Diehl and M. Cook, "Unsupervised learning of digit recognition using spike-timing-dependent plasticity," *Frontiers Comput. Neurosci.*, vol. 9, 2015, Art. no. 99.

[22] M. Pfeiffer, and T. Pfeil, "Deep learning with spiking neurons: opportunities and challenges," *Frontiers Neurosci.*, vol. 12, Oct. 2018, Art. no. 774.

[23] A. Tavanaei, M. Ghodrati, S. R. Kheradpisheh, T. Masquelier, and A. S. Maida, "Deep learning in spiking neural networks," *Neural Netw.*, vol. 111, pp. 47–63, 2019

[24] A. Taherkhani, A. Belatreche, Y. Li, G. Cosma, L. P. Maguire, T. M. McGinnity, "A review of learning in biologically plausible spiking neural networks," *Neural Netw.*, vol. 122, pp. 253–272, 2020.

[25] C. Mead, "Neuromorphic electronic systems," *Proc. IEEE*, vol. 78, no. 10, pp. 1629–1636, Oct. 1990.

[26] D. Ma *et al.*, "Darwin: a neuromorphic hardware co-processor based on spiking neural networks," *Sci. China Inform. Sci.*, vol. 59, no. 2, pp. 1–5, Feb. 2016.

[27] C. Li *et al.*, "Efficient and self-adaptive in-situ learning in multilayer memristor neural networks," *Nat. Commun.*, vol. 9, Jun. 2018, Art. no. 2385.

[28] Z. R. Wang *et al.*, "Fully memristive neural networks for pattern classification with unsupervised learning," *Nat. Electron.*, vol. 1, pp. 137–145, Feb. 2018.

[29] I. Boybat *et al.*, "Neuromorphic computing with multi-memristive synapses," *Nat. Commun.* vol. 9, Jun. 2018, Art. no. 2514.

[30] M. Davies *et al.*, "Loihi: A neuromorphic manycore processor with on-chip learning," *IEEE Micro*, vol. 38, no. 1, pp. 82–99, Jan./Feb. 2018.

[31] Q. Xia and J. J. Yang, "Memristive crossbar arrays for brain-inspired computing," *Nat. Mater.* vol. 18, pp. 309–323, Apr. 2019.

[32] J. Pei *et al.*, "Towards artificial general intelligence with hybrid Tianjic chip architecture," *Nature*, vol. 572, pp. 106–111, Jul. 2019.

[33] A. Hurtado, I. D. Henning, and M. J. Adams, "Optical neuron using polarization switching in a 1550 nm-VCSEL," *Opt. Express*, vol. 18, no. 24, pp. 25170–25176, Nov. 2010.

[34] A. Hurtado, K. Schires, I. Henning, and M. Adams, "Investigation of vertical cavity surface emitting laser dynamics for neuromorphic photonic systems," *Appl. Phys. Lett.*, vol. 100, no. 10, pp. 103703–103703, Mar. 2012.

[35] M. P. Fok, Y. Tian, D. Rosenbluth, and P. R. Prucnal, "Pulse lead/lag timing detection for adaptive feedback and control based on optical spike-timing-dependent plasticity," *Opt. Lett.*, vol. 38, no. 4, pp. 419–421, Feb. 2013.

[36] M. A. Nahmias, B. J. Shastri, A. N. Tait, and P. R. Prucnal, "A leaky integrate-and-fire laser neuron for ultrafast cognitive computing," *IEEE J. Sel. Top. Quantum Electron.*, vol. 19, no. 5, Sep./Oct. 2013, Art. no. 1800212.

[37] F. Selmi, R. Braive, G. Beaudoin, I. Sagnes, R. Kuszelewicz, and S. Barbay, "Relative refractory period in an excitable semiconductor laser," *Phys. Rev. Lett.*, vol. 112, no. 18, May 2014, Art. no.183902.

[38] R. Toole and M. P. Fok, "Photonic implementation of a neuronal algorithm applicable towards angle of arrival detection and localization," *Opt. Express*, vol. 23, no. 12, pp. 16133–16141, Jun. 2015.

[39] Q. Ren, Y. Zhang, R. Wang, and J. Zhao, "Optical spike-timing-dependent plasticity with weight-dependent learning window and reward modulation," *Opt. Express*, vol. 23, no. 19, pp. 25247–25258, Sep. 2015.

[40] R. Toole *et al.*, "Photonic implementation of spike-timing-dependent plasticity and learning algorithms of biological neural systems," *J. Lightw. Technol.*, vol. 34, no. 2, pp. 470–476, Jan. 2016.

[41] P. R. Prucnal, B. J. Shastri, T. F. de Lima, M. A. Nahmias, and A. N. Tait, "Recent progress in semiconductor excitable lasers for photonic spike processing," *Adv. Opt. Photon.*, vol. 8, no. 2, pp. 228–299, May 2016.

[42] J. Robertson, T. Deng, J. Javaloyes, and A. Hurtado, "Controlled inhibition of spiking dynamics in VCSELs for neuromorphic photonics: Theory and experiments," *Opt. Lett.*, vol. 42, no. 8, pp. 1560–1563, Apr. 2017.

[43] Z. Cheng, C. Ríos, W. H. P. Pernice, C. D. Wright, and H. Bhaskaran, "On-chip photonic synapse," *Sci. Adv.*, vol. 3, no. 9, Sep. 2017, Paper e1700160.

[44] S. Y. Xiang *et al.*, "Cascadable neuron-like spiking dynamics in coupled VCSELs subject to orthogonally polarized optical pulse injection," *IEEE J. Sel. Top. Quantum Electron.*, vol. 23, no. 6, Nov./Dec. 2017, Art. no. 1700207.

[45] T. Deng, J. Robertson, and A. Hurtado, "Controlled propagation of spiking dynamics in vertical-cavity surface-emitting lasers: towards neuromorphic photonic networks," *IEEE J. Sel. Top. Quantum Electron.*, vol. 23, no. 6, Nov./Dec. 2017, Art. no. 1800408.
[46] T. Deng *et al.*, "Stable propagation of inhibited spiking dynamics in vertical-cavity surface-emitting lasers for neuromorphic photonic networks," *IEEE Access*, vol. 6, pp. 67951–67958, Oct. 2018.
[47] S. Y. Xiang, Y. H. Zhang, X. X. Guo, A. J. Wen, and Y. Hao, "Photonic generation of neuron-like dynamics using VCSELs subject to double polarized optical injection," *J. Lightw. Technol.*, vol. 36, no. 19, pp. 4227–4234, Mar. 2018.
[48] Y. H. Zhang, S. Y. Xiang, X. X. Guo, A. J. Wen, and Y. Hao, "Polarization-resolved and polarization-multiplexed spike encoding properties in photonic neuron based on VCSEL-SA," *Sci. Rep.*, vol. 8, Oct. 2018, Art. no. 16095.
[49] S. Y. Xiang, J. K. Gong, Y. H. Zhang, X. X. Guo, A. Wen, and Y. Hao, "Numerical implementation of wavelength-dependent photonic spike timing dependent plasticity based on VCSOA," *IEEE J. Quantum Electron.*, vol. 54, no. 6, Dec. 2018, Art. no. 8100107.
[50] I. Chakraborty, G. Saha, and K. Roy, "Photonic in-memory computing primitive for spiking neural networks using phase-change materials," *Phys. Rev. Appl.*, vol. 11, no. 1, Jan. 2019, Art. no. 014063.
[51] J. K. George *et al.*, "Neuromorphic photonics with electro-absorption modulators," *Opt. Express*, vol. 27, no. 4, pp. 5181–5191, Feb. 2019.
[52] C. Ríos1 *et al.*, "In-memory computing on a photonic platform," *Sci. Adv.*, vol. 5, Feb. 2019, Paper eaau5759.
[53] T. F. de Lima *et al.*, "Machine learning with neuromorphic photonics," *J. Lightw. Technol.*, vol. 37, no. 5, pp. 1515–1534, Mar 2019.
[54] Y. Zhang, S. Y. Xiang, X. Guo, A. Wen, and Y. Hao, "All-optical inhibitory dynamics in photonic neuron based on polarization mode competition in a VCSEL with an embedded saturable absorber," *Opt. Lett.*, vol. 44, no. 7, pp. 1548–1551, Apr. 2019.
[55] J. Feldmann, N. Youngblood, C. D. Wright, H. Bhaskaran, and W. H. P. Pernice1, "All-optical spiking neurosynaptic networks with self-learning capabilities," *Nature*, vol. 569, pp. 208–215, May 2019.
[56] A. N. Tait *et al.*, "Silicon photonic modulator neuron," *Phys. Rev. Appl.*, vol. 11, Jun. 2019, Art. no. 064043.
[57] S. Y. Xiang, Y. Zhang, J. Gong, X. Guo, L. Lin, and Y. Hao, "STDP-based unsupervised spike pattern learning in a photonic spiking neural network with VCSELs and VCSOAs," *IEEE J. Sel. Top. Quantum Electron.*, vol. 25, no. 6, Nov./Dec. 2019, Art. no. 1700109.
[58] V. A. Pammi, K. Alfaro-Bittner, M. G. Clerc, and S. Barbay, "Photonic computing with single and coupled spiking micropillar lasers," *IEEE J. Sel. Top. Quantum Electron.*, vol. 26, no. 1, Jan./Feb. 2020, Art. no. 1500307.
[59] J. Robertson, E. Wade, Y. Kopp, J. Bueno, and A. Hurtado, "Toward neuromorphic photonic networks of ultrafast spiking laser neurons," *IEEE J. Sel. Top. Quantum Electron.*, vol. 26, no. 1, Jan./Feb. 2020, Art. no. 7700715.
[60] H. -T. Peng *et al.*, "Temporal information processing with an integrated laser neuron," *IEEE J. Sel. Top. Quantum Electron.*, vol. 26, no. 1, Jan./Feb. 2020, Art. no. 5100209.
[61] S. Y. Xiang, Z. Ren, Y. Zhang, Z. Song, and Y. Hao, "All-optical neuromorphic XOR operation with inhibitory dynamics of a single photonic spiking neuron based on VCSEL-SA," *Opt. Lett.*, vol. 45, no. 5, pp. 1104–1107, Mar. 2020.
[62] M. Hejda, J. Robertson, J. Bueno, and A. Hurtado, "VCSELs for fast neuromorphic photonic systems operating at GHz rates," *OFC*, Mar. 2020, Paper T4C.1.
[63] S. Xiang *et al.*, "Hardware architecture and algorithm co-design for multi-layer photonic neuromorphic network with excitable VCSELs-SA," *OFC*, Mar. 2020, Paper W3A.1.
[64] J. Robertson, M. Hejda, J. Bueno, and A. Hurtado, "Ultrafast optical integration and pattern classification for neuromorphic photonics based on spiking VCSEL neurons," *Sci. Rep.*, vol. 10, Apr. 2020, Art. no. 6098.
[65] Z. W. Song, S. Y. Xiang, Z. X. Ren, G. Q. Han, and Y. Hao, "Spike sequence learning in a photonic spiking neural network consisting of VCSELs-SA with supervised training," *IEEE J. Sel. Top. Quantum Electron.*, vol. 26, no. 5, Sep./Oct. 2020, Art. no. 1700209.
[66] Y. Nishitani, Y. Kaneko, and M. Ueda, "Supervised learning using spike-timing-dependent plasticity of memristive synapses," *IEEE Trans. Neural Netw. Learn. Syst.*, vol. 26, no. 12, pp. 2999–3008, Dec. 2015.
[67] Q. Yu, R. Yan, H. Tang, K. C. Tan, and H. Li, "A spiking neural network system for robust sequence recognition," *IEEE Trans. Neural Netw. Learn. Syst.*, vol. 27, no. 3, pp. 621–635, Mar. 2016.
[68] M. Fok, "A review: Neural-inspired photonic functional systems for dynamic RF signal processing," *J. Lightw. Technol.*, to be published, doi: 10.1109/JLT.2020.2993292.
[69] M. Yamada, "A theoretical analysis of self-sustained pulsation phenomena in narrow-stripe semiconductor lasers," *IEEE J. Quantum Electron.*, vol. 29, no. 5, pp. 1330–1336, May 1993.
[70] M. San Miguel, Q. Feng, and J. V. Moloney, "Light polarization dynamics in surface-emitting semiconductor lasers," *Phys. Rev. A*, vol. 52, no. 2, pp. 1728–1739, 1995.
[71] A. Scirè, J. Mulet, C. R. Mirasso, and M. San Miguel, "Intensity and polarization self-pulsations in vertical-cavity surface-emitting lasers," *Opt. Lett.*, vol. 27, no. 6, pp. 391–393, Mar. 2002.

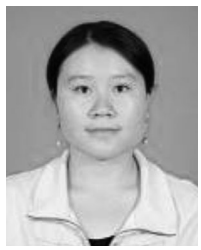

Shuiying Xiang was born in Ji'an, China, in 1986. She received the Ph.D. degree from Southwest Jiaotong University, Chengdu, China, in 2013.

She is currently a Professor with State Key Laboratory of Integrated Service Networks, Xidian University, Xi'an, China. She is the author or coauthor of more than 100 research papers. Her research interests include neuromorphic photonics and semiconductor lasers dynamics.

Zhenxing Ren was born in Baoji, China, in 1996. He is currently working toward the master's degree from Xidian University, Xi'an, China. His researching interest is machine learning, spiking neural network.

Yahui Zhang was born in Zhangjiakou, China, in 1993. She is currently working toward the Ph.D. degree from Xidian University, Xi'an, China. Her researching interest is the vertical cavity surface-emitting lasers, neuromorphic photonic systems, brain-inspired information processing, spiking neural network

Ziwei Song was born in Jiaozuo, China, in 1996. She is currently working toward the master's degree from Xidian University, Xi'an, China. Her researching interest is the vertical cavity surface-emitting lasers, neuromorphic photonic systems.

Xingxing Guo was born in Ji'an, China, in 1993. She is currently working toward the M.S. degree from Xidian University, Xi'an, China. Her researching interest is the dynamics and applications of semiconductor lasers.

Genquan Han was born in Hengshui, China, in 1979. He received the B.Eng. degree from Tsinghua University, Beijing, China, and the Ph.D. degree from the Institute of Semiconductors, Chinese Academy of Sciences, Beijing, in 2008.

He is currently a Professor with Xidian University, Xi'an, China. His current research interests include advanced CMOS, photonics devices, and wide bandgap materials and devices.

Yue Hao was born in the city of Chongqing, China, in 1958. He received the Ph.D. degree from Xi'an Jiao tong University, Xi'an, China, in 1991.

He is currently a Professor at State Key Discipline Laboratory of Wide Bandgap Semiconductor Technology, the School of Microelectronics, Xidian University, Xi'an. His research interests include wide forbidden band semiconductor materials and devices.